nature plants

ARTICLES

https://doi.org/10.1038/s41477-017-0095-4

Control of auxin-induced callus formation by bZIP59–LBD complex in *Arabidopsis* regeneration

Chongyi Xu[1], Huifen Cao[1,2], Qianqian Zhang[1], Hongzhe Wang[1], Wei Xin[1], Enjun Xu[1], Shiqi Zhang[1,2], Ruixue Yu[1,2], Dongxue Yu[1,2] and Yuxin Hu[1,3]*

Induction of pluripotent cells termed callus by auxin represents a typical cell fate change required for plant in vitro regeneration; however, the molecular control of auxin-induced callus formation is largely elusive. We previously identified four *Arabidopsis* auxin-inducible Lateral Organ Boundaries Domain (LBD) transcription factors that govern callus formation. Here, we report that *Arabidopsis* basic region/leucine zipper motif 59 (AtbZIP59) transcription factor forms complexes with LBDs to direct auxin-induced callus formation. We show that auxin stabilizes AtbZIP59 and enhances its interaction with LBD, and that disruption of *AtbZIP59* dampens auxin-induced callus formation whereas overexpression of *AtbZIP59* triggers autonomous callus formation. AtbZIP59–LBD16 directly targets a *FAD-binding Berberine* (*FAD-BD*) gene and promotes its transcription, which contributes to callus formation. These findings define the AtbZIP59–LBD complex as a critical regulator of auxin-induced cell fate change during callus formation, which provides a new insight into the molecular regulation of plant regeneration and possible developmental programs.

Detached organs or tissues of plants have a remarkable capacity to regenerate new organs or entire new individuals under the appropriate culture conditions[1,2]. In a typical plant in vitro regeneration system, the regeneration experiment often starts with the induction of pluripotent cells named callus from explants cultivated on an auxin-rich callus-inducing medium (CIM), and the subsequent regeneration of shoots or roots can be triggered by incubating the callus cells on a cytokinin-rich shoot-inducing medium or an auxin-rich root-inducing medium, respectively[3,4]. Therefore, it is believed that auxin-induced callus formation represents a typical cell fate change in which some somatic cells acquire pluripotency[3,5], and that auxin and cytokinin play critical roles in the determination of the regenerating fates of plant cells[3,6]. Although this auxin–cytokinin paradigm has become the foundation of a large number of in vitro regeneration systems in a variety of plant species and an invaluable biotechnology for agricultural application for over a half-century[7,8], the molecular mechanisms regulating plant cell fates during regeneration are largely elusive.

Recent studies in *Arabidopsis* have begun to reveal the molecular basis behind cell fate change during plant regeneration. In *Arabidopsis*, auxin-induced callus formation in multiple organs actually occurs from the pericycle and pericycle-like cells, and the derived calluses resemble the root meristem by ectopic expression of key regulators of the root meristem, suggesting that auxin-induced callus formation shares some characteristics of a root developmental pathway[4,9–11]. Indeed, the mutation of *Aberrant Lateral Root Formation 4* (*ALF4*), which severely blocks the initial division of pericycle cells, significantly inhibits the callus-forming capability of multiple organs on CIM[10]. Consistent with this, specific ablation of pericycle cell function with diphtheria toxin chain A abrogates both lateral root formation and auxin-induced callus formation[11,12]. Furthermore, the four auxin-inducible LBD transcription factors LBD16, LBD17, LBD18 and LBD29 that function downstream of AUXIN RESPONSE FACTOR7 (ARF7) and ARF19 to mediate the lateral root formation[13,14] are found to play a critical role in directing auxin-induced callus formation in regeneration program[15]. Recently, the auxin-induced lateral root primordia at appropriate stages have been found to be required for their subsequent conversion into the shoot apical meristems on shoot-inducing medium in *Arabidopsis*[16]. By contrast, the wound-triggered callus formation at wounding sites is found to be directed by the APETALA2/ETHYLENE RESPONSIVE ELEMENT BINDING FACTOR (AP2/ERF) transcription factors, WOUND INDUCED DEDIFFERENTIATION 1–4 (WIND1–4)[17]. Although a recent transcriptomic analysis shows that some wound-induced genes are found to be highly expressed in auxin-induced callus formation[18], the WIND-directed callus formation appears not to follow the root developmental program but depends on the activation of ARABIDOPSIS RESPONSE REGULATOR (ARR)-dependent cytokinin signalling, suggesting that wound-triggered callus formation might be via a pathway of cell dedifferentiation[17,18].

The *Arabidopsis* basic region/leucine zipper motif (bZIP) transcription factor represents a large family of transcription factors[19], which has been shown to be involved in pathogen defence, light-induced signalling, seed maturation and flower development[19,20]. One domain of the bZIP protein is involved in DNA binding while the other leucine zipper motif determines the dimerization specificity[19, 21,22]. The *Arabidopsis* bZIP transcription factors are classified into ten groups[19], among which the AtbZIP59 (also designated as ANTHOCYANIN-IMPAIRED RESPONSE-1, AIR1), a member of the group I bZIP subfamily, has been shown to be involved in osmosensory responses and regulation of anthocyanin biosynthesis during salt stress[23,24]. Here, we report that the AtbZIP59 acts as a partner of LBDs to mediate the auxin-induced callus formation. Our findings thus define the AtbZIP59–LBD complex as a critical regulator of auxin-directed cell fate change during in vitro regeneration and possible developmental programs in plants.

[1]Key Laboratory of Plant Molecular Physiology, CAS Center for Excellence in Molecular Plant Sciences, Institute of Botany, Chinese Academy of Sciences, Beijing, China. [2]University of Chinese Academy of Sciences, Beijing, China. [3]National Center for Plant Gene Research, Beijing, China. *e-mail: huyuxin@ibcas.ac.cn

Results

AtbZIP59 physically interacts with LBD16, LBD17 and LBD29. We previously demonstrated that the four *Arabidopsis* LBD transcription factors (LBD16, LBD17, LBD18 and LBD29) act downstream of ARF7 and ARF19 to direct auxin-induced callus formation[15]. To gain further insight into the molecular control of auxin-induced callus formation, we used LBD17 as a bait and performed a yeast two-hybrid screen with a complementary DNA library constructed with messenger RNA isolated from aerial and root explants incubated on CIM for 12, 24 and 48 h. This screening allowed us to identify a few candidate proteins including AtbZIP59 that could interact with LBD17. A further pairwise experiment validated the interaction of AtbZIP59 and LBD17 in the yeast two-hybrid assay (Fig. 1a). To test whether AtbZIP59 could physically interact with LBDs in planta, we first carried out a co-immunoprecipitation (co-IP) experiment in *Nicotiana benthamiana* leaves transiently expressing AtbZIP59–MYC and/or LBD16–GFP, LBD17–GFP and LBD29–GFP, respectively. The co-IP assays revealed that AtbZIP59 could be immunoprecipitated by LBD16, LBD17 and LBD29 (Fig. 1b). Next, we tested these interactions by a bimolecular fluorescence complementation (BiFC) assay[25]. Co-expression of LBD16, LBD17 or LBD29 fused with the amino terminus of the yellow fluorescent protein (YFP^N) and AtbZIP59 fused with the carboxy terminus of YFP (YFP^C) in *N. benthamiana* clearly showed that AtbZIP59 could physically interact with auxin-inducible LBD16, LBD17 and LBD29 in the nucleus of epidermal cells of *N. benthamiana* leaves (Fig. 1c), confirming the interaction of AtbZIP59 with auxin-inducible LBDs in planta.

AtbZIP59 mediates auxin-induced callus formation. To examine whether AtbZIP59, as a partner of LBDs, is also involved in directing auxin-induced callus formation, we obtained a transfer DNA (T-DNA) insertion mutant of *AtbZIP59*, previously named *air1-2* (SALK_024459)[24], in which a T-DNA fragment was inserted into the first exon of *AtbZIP59*, resulting in a transcriptional null mutant allele of *AtbZIP59* (Supplementary Fig. 1a,b). Compared with the wild type (WT), the *air1-2* aerial organs did not show obvious developmental defects under normal growth condition (Supplementary Fig. 1c). However, when the *air1-2* seedlings were incubated on CIM, the callus-forming capacity of *air1-2* roots was clearly dampened in comparison to that of the WT (Fig. 2a,b). Moreover, the introduction of a *ProAtbZIP59::AtbZIP59–GFP* construct into *air1-2* could fully restore the compromised callus-forming phenotype (Fig. 2a,b and Supplementary Fig. 1d), demonstrating that *AtbZIP59* is responsible for the compromised callus-forming phenotype of *air1-2*. Since auxin-induced lateral root initiation and callus formation share some characteristics of a root developmental program[15], we also examined whether disruption of *AtbZIP59* affects the lateral root initiation. As expected, *air1-2* seedlings on Murashige and Skoog (MS) medium had a reduced number of lateral roots when compared with the WT, and this phenotype was rescued in the *ProAtbZIP59::AtbZIP59–GFP air1-2* seedlings (Supplementary Fig. 1e). In addition, the *air1-2* seedlings were hyposensitive to exogenous auxin regarding the lateral root initiation (Supplementary Fig. 1e). These results demonstrate that *AtbZIP59* is involved in auxin-induced callus formation and lateral root initiation.

Next, we overexpressed *AtbZIP59–MYC* under the control of the cauliflower mosaic virus 35S promoter (*Pro35S::AtbZIP59-MYC*) in *Arabidopsis* to test whether ectopic expression of *AtbZIP59* could trigger autonomous callus formation like that of *LBDs*[15]. As expected, we observed that T1 transgenic *Pro35S::AtbZIP59-MYC* seedlings grown on B5 medium without any exogenous phytohormone exhibited various degrees of the autonomous callus-forming phenotype (Fig. 2c). Among 450 individuals examined, ~5% of seedlings displayed complete conversion of leaves into calluses (strong), ~15% of seedlings developed calluses in their hypocotyls (intermediate) and ~80% of seedlings formed visible calluses in their roots (weak) (Fig. 2d). Moreover, immunoblotting analysis of different transgenic lines showed a close correlation between the strength of phenotype and the abundances of ectopically expressed AtbZIP59 (Fig. 2e), confirming that ectopic expression of *AtbZIP59* is sufficient to trigger callus formation without exogenous phytohormone. Similarly to the observations in transgenic *LBD* plants[15], only the transgenic *Pro35S::AtbZIP59–MYC* plants with the weak phenotype could produce T2 progenies, and the autonomous callus formation still occurred in the roots or aerial organs of these T2 plants grown

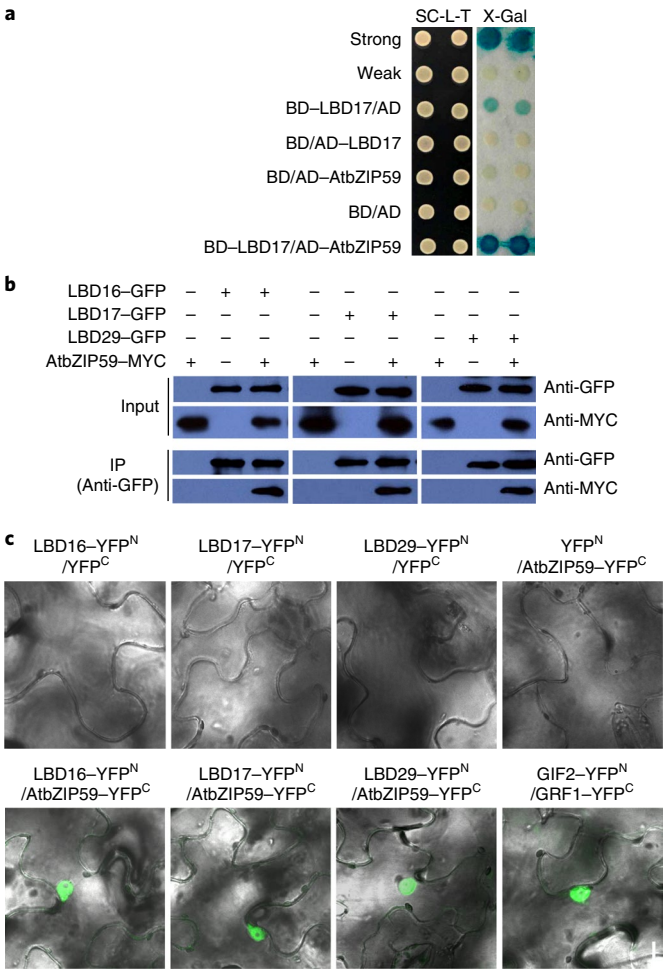

Fig. 1 | AtbZIP59 physically interacts with auxin-inducible LBDs. a, Interaction of AtbZIP59 and LBD17 in a yeast two-hybrid assay. Yeasts were grown on Synthetic Complete-Leu-Trp (SC-L-T) medium and the interaction of AD–AtbZIP59 with BD–LBD17 was assayed by the reporter gene *LacZ* (X-Gal). The pairwise rat Krev1–RalGDS-wt (Strong) and rat Krev1–RalGDS-m1 (Weak) were used as a strong and weak positive control, respectively. **b**, Interactions of AtbZIP59 with LBD16, LBD17 and LBD29 assayed by co-IP. The transiently expressed LBD–GFP and/or AtbZIP59 in *N. benthamiana* leaves was immunoprecipitated using an agarose-conjugated anti-GFP matrix and immunoblotted by anti-GFP and/or anti-MYC antibody. The experiments were performed in three biological replicates. **c**, Bimolecular fluorescence complementation assayed interactions of AtbZIP59 and LBD16, LBD17 and LBD29. LBD16, LBD17 and LBD29 fused with the N-terminal fragment of YFP (YFP^N) and/or AtbZIP59 fused with the C-terminal fragment of YFP (YFP^C) were infiltrated into *N. benthamiana* leaves for three days, and YFP fluorescence was visualized in the epidermal cells under a confocal microscope. The interaction of GIF2 and GRF1 was used as a positive control. Scale bar, 10 μm.

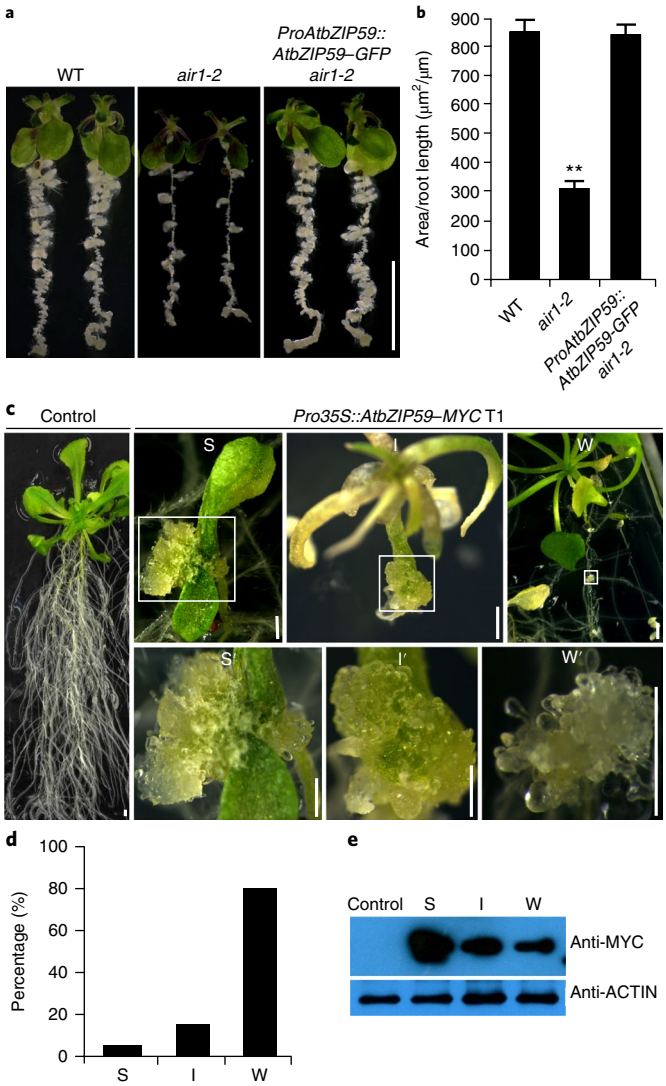

Fig. 2 | *AtbZIP59* mediates auxin-inducible callus formation. a,**b**, The callus-forming phenotype of WT, *air1-2* and *air1-2* plants carrying a *ProAtbZIP59::AtbZIP59–GFP* construct (*ProAtbZIP59::AtbZIP59–GFP air1-2*). The five-day-old seedlings were incubated on CIM containing 0.2 mg l^{-1} 2,4-D for nine days (**a**), and the area of pericycle or pericycle-derived calluses in the primary roots was quantified at 4 days (**b**). Scale bar, 5 mm. Data are shown as mean ± s.d. ($n = 20$, $^{**}P < 0.01$; Student's *t*-test). **c**, The autonomous callus-forming phenotypes of strong (S), intermediate (I) and weak (W) *Pro35S::AtbZIP59–MYC* T1 seedlings. The recovered transgenic seedlings harbouring an empty vector (Control) or *Pro35S::AtbZIP59–MYC* construct were grown on hormone-free B5 medium for 30 days. S′, I′ and W′ show enlarged images of the areas outlined by the rectangles. Scale bars, 1 mm. **d**, Percentages of transgenic *Pro35S::AtbZIP59–MYC* seedlings with the S, I or W phenotype described in **c**. About 450 transgenic *Pro35S::AtbZIP59–MYC* T1 seedlings were examined for their autonomous callus-forming phenotype. **e**, AtbZIP59–MYC levels of transgenic *Pro35S::AtbZIP59–MYC* seedlings with the S, I or W phenotype.

on medium without exogenous phytohormone (Supplementary Fig. 2). Moreover, the ectopic activation of root stem cell markers PLETHORA 1 (PLT1) and WUSCHEL-RELATED HOMEOBOX 5 (WOX5) was observed in the callusing hypocotyls and leaves of these *Pro35S::AtbZIP59–MYC* seedlings (Supplementary Fig. 3), demonstrating that AtbZIP59-triggered callus formation is via a root developmental program.

Auxin stabilizes AtbZIP59 and enhances its interaction with LBD. To investigate the tissue-specific expression of *AtbZIP59*, we generated transgenic *Arabidopsis* plants harbouring a *ProAtbZIP59::GUS* transgene. A GUS staining assay revealed that *AtbZIP59* seemed to be ubiquitously expressed in cotyledons, juvenile leaves and roots, but strongly expressed in the vascular cylinder (stele) of roots and vasculature of cotyledons and leaves (Supplementary Fig. 4a–d). Next, we examined the AtbZIP59 accumulation with *ProAtbZIP59::AtbZIP59–GFP air1-2* seedlings. The GFP fluorescence signal appeared to be visualized ubiquitously but predominantly in the pericycle and pericycle-like cells of cotyledon petiole, hypocotyl, root and in lateral root primordia (Supplementary Fig. 4e–i). Consistent with the previous finding that the C-terminal bZIP domain of AtbZIP59 contains the nuclear localization signal and nuclear export signal[23], AtbZIP59 was found to be dually localized into the cytosol and nucleus of cells (Supplementary Fig. 4e–i).

Next, we examined the transcription of *AtbZIP59* in response to CIM treatments. Surprisingly, both real-time quantitative reverse transcription PCR (qRT–PCR) analysis in WT plants and the GUS staining assay in the *ProAtbZIP59::GUS* plants showed that *AtbZIP59* transcription was decreased after the seedlings were incubated on CIM (Fig. 3a,b). Nevertheless, further immunoblotting analysis of the *ProAtbZIP59::AtbZIP59–GFP air1-2* seedlings revealed that AtbZIP59 abundance was significantly elevated after seedlings were incubated on CIM or treated with auxin (Fig. 3c and Supplementary Fig. 5a), indicating that auxin regulates AtbZIP59 accumulation at the post-transcriptional level. To explore whether auxin affects AtbZIP59 protein synthesis or stability, we incubated the transgenic *ProAtbZIP59::AtbZIP59–GFP air1-2* seedlings on CIM supplemented with the protein synthetic inhibitor cycloheximide (CHX) or the proteasome inhibitor MG132, respectively. We found that inhibition of protein synthesis did not block the induction of AtbZIP59 by CIM, while treatment with MG132 caused abundant AtbZIP59 accumulation in the seedlings incubated either on hormone-free medium or on CIM (Fig. 3c and Supplementary Fig. 5a). These observations strongly suggest that auxin regulates AtbZIP59 accumulation by affecting protein stability.

To investigate the cellular basis of AtbZIP59 and LBD in directing callus formation, we examined the tissue-specific accumulation of AtbZIP59 and LBD16 by incubating the transgenic *ProAtbZIP59::AtbZIP59–GFP air1-2* and *ProLBD16::LBD16–GFP lbd16-2* seedlings on CIM. Although the GFP signal of AtbZIP59–GFP appeared to be expressed ubiquitously in all of the cell types before CIM incubation, a dramatic accumulation of AtbZIP59 in the pericycle or pericycle-like cells of root and aerial organs was observed on activation of callus formation by CIM (Fig. 3d). Similarly, the GFP fluorescence signal of LBD16–GFP was strongly induced by CIM in the pericycle and pericycle-like cells of these organs where the callus was actively formed (Supplementary Fig. 5b), supporting that AtbZIP59 acts as a partner of LBD to direct pericycle or pericycle-like cells to form a callus. To test whether CIM could affect the AtbZIP59 and LBD16 interaction, we conducted co-IP experiments with transgenic plants overexpressing *Pro35S::AtbZIP59–MYC* and/or *Super::LBD16–FLAG* before and after being incubated on CIM. Careful examination of a parallel co-IP assay showed that the precipitation efficiency of LBD16 by AtbZIP59 was enhanced by CIM treatment (Fig. 3e). These observations strengthen the idea that AtbZIP59 and auxin-inducible LBD form a complex to direct the fate changes of pericycle or pericycle-like cells during auxin-induced callus formation.

AtbZIP59 and LBD16 act synergistically in directing cell fate. To further explore the interactive role of AtbZIP59 and LBD in auxin-induced callus formation, we generated a *lbd16-2 air1-2* double mutant and examined its callus-forming capacity. Compared to the dampened callus-forming phenotype of *lbd16-2* and *air1-2* roots,

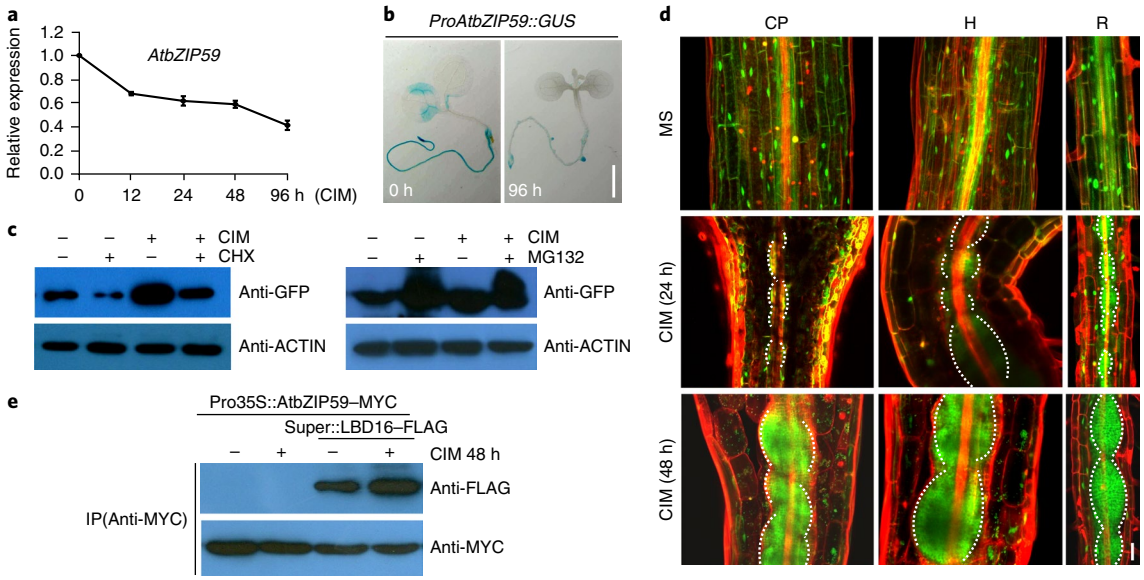

Fig. 3 | CIM stabilizes AtbZIP59 and enhances its interaction with LBD16. a,**b**, *AtbZIP59* transcription was downregulated by CIM. **a**, qRT–PCR analysis of *AtbZIP59* expression was performed with seven-day-old WT seedlings on CIM for 0, 12, 24, 48 and 96 h, and the data from three biological replicates are shown as mean ± s.d. **b**, The GUS-staining assay was carried out with transgenic *ProAtbZIP59::GUS* seedlings before and after being incubated on CIM for 96 h. Scale bar, 2 mm. **c**, CIM stabilizes the AtbZIP59 protein. Immunoblot assays were performed with seven-day-old *ProAtbZIP59::AtbZIP59–GFP air1-2* seedlings transferred into liquid B5 and CIM medium supplemented with or without 1 μM CHX, or 20 mM MG132 for 48 h, respectively. Total proteins were immunoblotted by anti-GFP and anti-ACTIN (loading control) antibodies, with three biological replicates. **d**, CIM-induced AtbZIP59 accumulation in pericycle and pericyle-like cells. GFP signals overlaid with signals of organs stained by propidium iodide (red) were visualized in five-day-old *ProAtbZIP59::AtbZIP59–GFP air1-2* seedlings before (MS) and after incubation on CIM for 24 h and 48 h. CP, cotyledon petiole; H, hypocotyl; R, root. Scale bars, 50 μm. **e**, CIM-enhanced interaction of AtbZIP59 and LBD16 in planta. Co-IP assays were performed in triplicate with transgenic *Pro35S::AtbZIP59–MYC* plants with or without a *Super::LBD16–FLAG* construct incubated on hormone-free medium or CIM for 48 h.

the callus-forming capacity in *lbd16-2 air1-2* roots was almost blocked (Fig. 4a,b). Similarly, the compromised callus-forming capacity in the cotyledon and hypocotyl of *lbd16-2* and *air1-2* plants was also enhanced in the *lbd16-2 air1-2* double mutant (Supplementary Fig. 6a). In addition, the lateral root number of *lbd16-2 air1-2* was dramatically reduced when compared to the single mutant (Supplementary Fig. 6b,c). These findings suggest that AtbZIP59 and LBD16 act synergistically in mediating callus formation and lateral root initiation. To verify this, we generated transgenic plants overexpressing *AtbZIP59* and *LBD16* by crossing a weak *Pro35S::AtbZIP59–MYC* line with a *Super::LBD16–FLAG* line. Although neither of the two parental lines exhibited any visibly autonomous callus-forming phenotype, the seven-day-old F1 seedlings displayed a dramatic phenotype with a complete arrest of development, in which the cotyledon cells were highly disorganized and the tight cell differentiations were disturbed (Fig. 4c,d), and these cotyledons then developed into callus-like organs on hormone-free medium (Fig. 4e). In addition, we also observed that disruption of *LBD16* or *AtbZIP59* in the transgenic *Pro35S::AtbZIP59–MYC* or *Pro35S::LBD16* greatly attenuated their spontaneous callus-forming phenotype, respectively (Supplementary Fig. 6d,e). Taking these results together, we concluded that AtbZIP59 and LBD act synergistically in directing cell fate change during callus formation and possibly in developmental programs.

***FAD-BD* is a direct target of the AtbZIP59–LBD16 complex.** Since AtbZIP59 and LBD could form a heterodimer, it is likely that they share a common downstream target to direct callus formation. A previous study showed that *FAD-BD*, which encodes a BBE-like enzyme involved in cell wall metabolism by catalysing the oxidation of monolignols[26], is a direct target of LBD16 in promoting lateral root emergence of *Arabidopsis*[27], and our transcriptomic analysis also revealed that *FAD-BD* was rapidly induced by CIM in roots and aerial organs in *Arabidopsis*[28]. We thus speculated that *FAD-BD* is probably targeted by the AtbZIP59–LBD16 complex and may contribute to callus formation. To test this, we first examined *FAD-BD* expression in *Super::LBD16–FLAG*, *Pro35S::AtbZIP59–MYC*, *lbd16-2*, *air1-2* and *air1-2 lbd16-2* plants, respectively. As expected, the transcript level of *FAD-BD* was found to be elevated by overexpression of *LBD16* or *AtbZIP59* but deceased in *lbd16-2*, *air1-2* and especially *air1-2 lbd16-2* plants when compared to that in the WT (Fig. 5a). Next, we generated transgenic plants overexpressing *FAD-BD*, and we observed that ~19% of seedlings had visibly autonomous calluses among the 132 *Pro35S::FAD-BD* transgenic T1 seedlings examined (Fig. 5b), suggesting that *FAD-BD* is a target of the LBD16–AtbZIP59 heterodimer and activation of *FAD-BD* contributes to auxin-induced callus formation.

We next tested whether the LBD16–AtbZIP59 complex could bind to the *FAD-BD* promoter region in planta in transgenic *ProLBD16::LBD16–GFP lbd16-2* and *ProAtbZIP59::AtbZIP59–GFP air1-2* seedlings after incubation on CIM. The quantitative real-time PCR analysis of the *FAD-BD* promoter fragments (F-1 to F-6) immunoprecipitated by GFP antibody clearly showed that both the F-1 and F-3 regions were apparently enriched in the *ProLBD16::LBD16–GFP lbd16-2* and *ProAtbZIP59::AtbZIP59–GFP air1-2* seedlings when compared with those in WT plants (Fig. 5c), showing that AtbZIP59 and LBD16 could bind to the same regions of the *FAD-BD* promoter. To examine whether AtbZIP59 and LBD16 could activate *FAD-BD* transcription, we co-transformed the *Pro35S::Ω:LBD16–GFP*, *Pro35S::Ω:AtbZIP59–GFP* or *Pro35S::GFP* effector plasmids with a *ProFAD-BD::LUC* (luciferase) reporter plasmid into *Arabidopsis* protoplasts and examined the activity of the LUC reporter. As expected, transiently expressed LBD16 or AtbZIP59 resulted in a significant increase of *ProFAD-BD-*

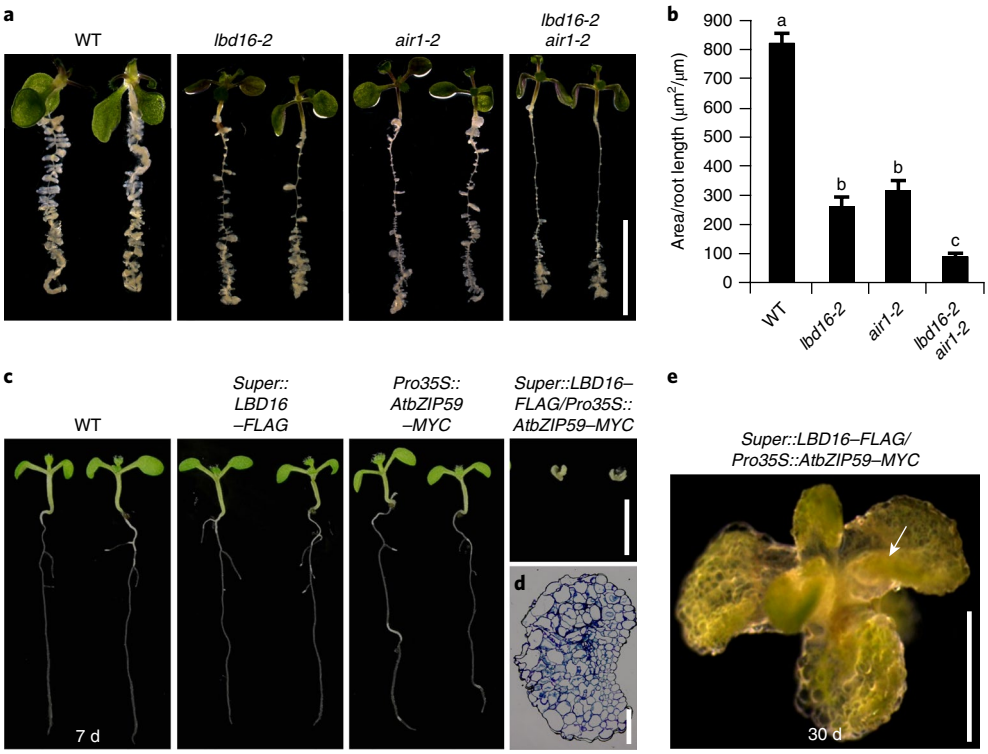

Fig. 4 | AtbZIP59 and LBD16 act synergistically in directing callus formation. a,**b**, The callus-forming phenotype and quantified callus area of five-day-old WT, *lbd16-2*, *air1-2* and *lbd16-2 air1-2* seedlings on CIM containing 0.2 mg l^{-1} 2,4-D for 9 days or 4 days. Callus area is shown as mean ± s.d. ($n = 20$, one-way analysis of variance test, and the letters a to c indicate significant differences between phenotypes ($P < 0.05$)). Scale bar, 10 mm. **c**, Morphology of the seven-day-old transgenic *Super::LBD16–FLAG*, *Pro35S::AtbZIP59–MYC* or *Super::LBD16–FLAG/Pro35S::AtbZIP59-MYC* F1 seedlings. Scale bar, 10 mm. **d**, Semi-thin section of the cotyledon of seven-day-old *Super::LBD16–FLAG/Pro35S::AtbZIP59–MYC* F1 seedling in the transverse direction. Scale bar, 40 μm. **e**, Morphology of a 30-day-old *Super::LBD16–FLAG/Pro35S::AtbZIP59-MYC* F1 seedling. The white arrow indicates a formed callus. Scale bar, 2 mm.

driven LUC activity when compared to the control effector, and co-expression of LBD16 and AtbZIP59 could enhance such activity (Fig. 5d), supporting that AtbZIP59 and LBD16 act synergistically to activate *FAD-BD* transcription. Taking these results together, we concluded that *FAD-BD* is a direct target of the AtbZIP59–LBD16 complex and contributes to auxin-induced cell fate change during callus formation or possible developmental events.

Discussion

The auxin-induced callus formation in plant in vitro regeneration represents a typical cell fate change where somatic cells are switched into pluripotent callus cells, which is, to some extent, analogous to the induction of pluripotent stem cells in animals. Although most of the already differentiated cells had long been considered to have the potential to become callus cells under appropriate in vitro conditions, recent studies in *Arabidopsis* revealed that auxin-induced callus formation in multiple organs occurs from pericycle or pericycle-like cells via a root development program[9,10]. We previously showed that auxin-induced ectopic expression of LBD transcription factors, including LBD16, LBD17, LBD18 and LBD29, is critical in regulating the formation of pluripotent callus cells[15]. Here, we further identified an *Arabidopsis* transcription factor, AtbZIP59, that could physically interact with LBDs to mediate auxin-induced callus formation. We showed that disruption of *AtbZIP59* dampened the callus-forming capacity, whereas overexpression of *AtbZIP59* resulted in autonomous callus formation in the absence of phytohormone. We also provided evidence that auxin or CIM could induce AtbZIP59 accumulation in pericycle and pericycle-like cells and enhance its interaction with LBD, which in turn triggered the fate change of pericycle or pericycle-like cells and thus callus formation. Although the detailed downstream molecular events of the AtbZIP59–LBD complex need to be further explored, our findings clearly define the AtbZIP59–LBD complex as an important regulator of auxin-induced callus formation during plant in vitro regeneration.

Recently, the *Arabidopsis* heterodimeric transcription factor complex ETHYLENE RESPONSE FACTOR115 (ERF115)–PHYTOCHROME A SIGNALTRANSDUCTION1 (PAT1) was reported to account for the high regenerative potential of damaged roots by activating its putative target gene *WIND1*[29]. Although wound-triggered callus formation does not seem to follow the root developmental pathway, it appears that the two identified pathways controlling callus formation in plant regeneration both involve the heterodimeric transcription factor complex. Interestingly, ectopic expression of cell-type-specific transcription factors in animals can reprogram differentiated cells into pluripotent cells[30], in which the two key transcription factors, Sox2 and Oct4, have been shown to work together to form a functional and physical partnership in the control of the self-renewal and pluripotency of embryonic stem cells and epiblast stem cells[31]. Therefore, it seems common that the transcription regulatory complex is critical for governing cell fate change in both kingdoms.

Since both bZIP and LBD are large transcription factor families that regulate many aspects of growth and development as well as the response to environmental cues[19], and multiple LBD members, including LBD16, LBD17, LBD18 and LBD29, have been shown to act redundantly and cooperatively to direct callus formation, it is likely that other AtbZIP members might also function in cooperation with AtbZIP59 to form heterodimers with different LBDs in multiple organs to orchestrate auxin-induced callus formation. This might explain why disruption of *AtbZIP59* causes only a dampened

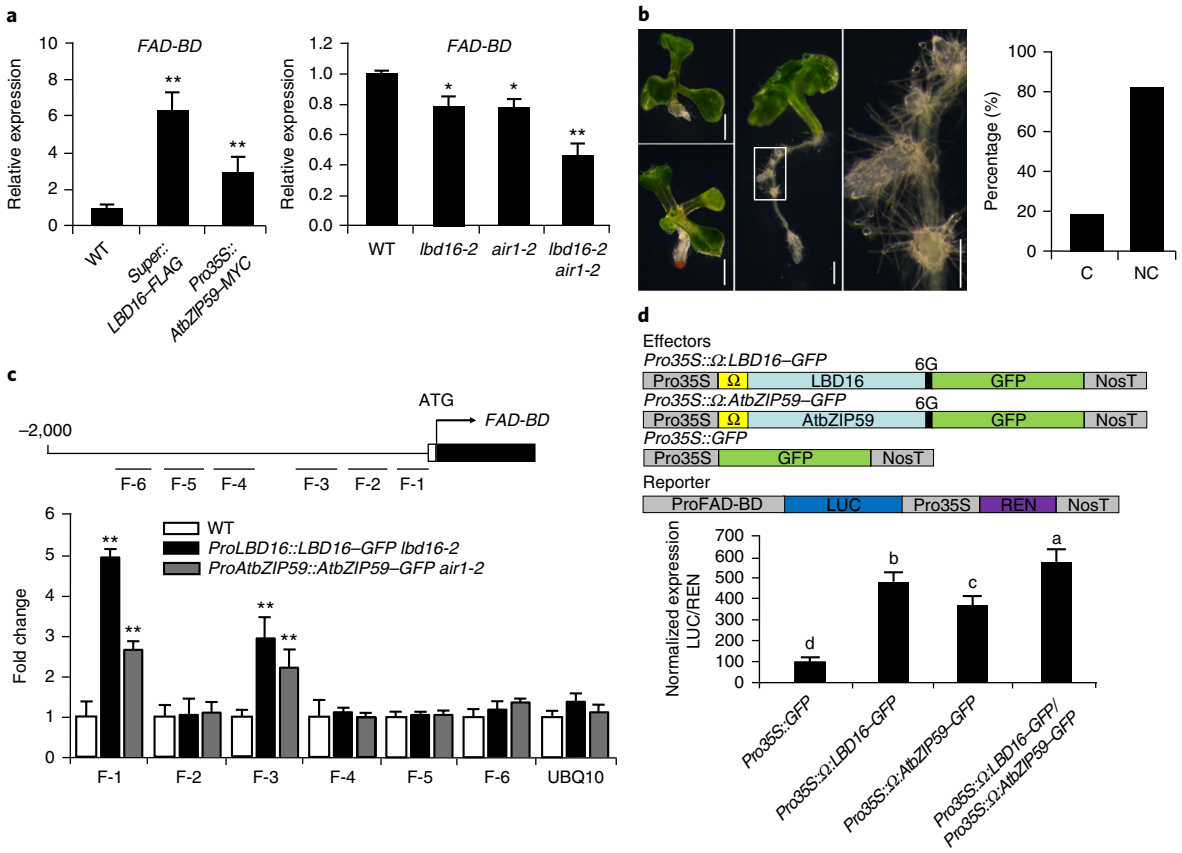

Fig. 5 | *FAD-BD* is targeted by the AtbZIP59–LBD16 complex. a, qRT–PCR analysis of *FAD-BD* expression in seven-day-old *Super::LBD16–FLAG* and *Pro35S::AtbZIP59–MYC* seedlings, and *lbd16-2*, *air1-2* and *lbd16-2 air1-2* seedlings. Data are shown as mean ± s.d. ($n = 3$ biological replicates, $^{**}P < 0.01$; $^{*}P < 0.05$; Student's *t*-test). **b**, Phenotype of 20-day-old transgenic *Pro35S::FAD-BD* T1 seedlings on hormone-free B5 medium. The right panel shows an enlarged image of the area outlined by the rectangle in the middle panel. Percentages of transgenic *Pro35S::FAD-BD* T1 seedlings with visible callus (C) and non-visible callus (NC) are shown in the right panel. Scale bars, 2 mm. **c**, ChIP–qPCR analysis of LBD16- and AtbZIP59-binding fragments (F-1 to F-6) in the *FAD-BD* promoter. *ProLBD16::LBD16–GFP lbd16-2* and *ProAtbZIP59::AtbZIP59–GFP air1-2* plants cultured in liquid CIM for 36 h were assayed by ChIP by anti-GFP antibody, and PCR primers used to amplify *FAD-BD* promoter regions F-1 to F-6 are indicated by black lines. A fragment of the *UBQ10* promoter was used as the negative control. Data from three independent replicates are shown as mean ± s.d. (Student's *t*-test, $^{**}P < 0.01$). **d**, LBD16 and AtbZIP59 synergistically activate *FAD-BD* transcription in the *Arabidopsis* protoplast. A diagram of the effector and reporter constructs used for transcriptional activity assays is shown in upper panel, Ω, a translational enhancer. The activity of the LUC reporter driven by the *FAD-BD* promoter was measured by assaying LUC/REN ratios. The activity of the LUC reporter in the *Arabidopsis* protoplast transformed with an empty vector was set to 100 for the control. Data from three independent replicates are shown as mean ± s.d. ($n = 3$, one-way analysis of variance test, $P < 0.05$).

callus-forming capacity of various organs and why AtbZIP59 and LBD16 have an additive role in directing callus formation. Moreover, since auxin is highly accumulated in pericycle and pericycle-like cells and also plays a role in lateral organ formation[32,33], it remains an open question whether AtbZIP–LBD complexes are involved in the maintenance of pericycle and pericycle-like cell states and/or the regulation of other cell fates during developmental programs. Therefore, our finding that the AtbZIP59–LBD complex is the critical regulator of auxin-induced cell fate change during callus formation may open a door to further explore the relationship between the remarkable plant regenerative capacity and developmental plasticity.

Methods

Plant materials. The *Arabidopsis thaliana* ecotype Columbia-0 was used in this study. The T-DNA insertion mutants *lbd16-2* (SALK_040739)[15] and *air1-2* (SALK_024459c)[24] were obtained from the Arabidopsis Biological Resource Center and verified by PCR analyses. *ProWOX5::GFP–ER* and *ProPLT1::PLT1–YFP* marker lines have been described previously[34,35].

Plant growth conditions. The *Arabidopsis* seeds were sterilized and germinated on half-strength Murashige and Skoog medium (1/2 MS: 1/2 MS medium, 1% sucrose, 0.55% plant agar, pH 5.7) at 22 ± 2 °C under long-day conditions (16 h light and 8 h dark) with an illumination intensity of 80–90 μmol m^{-2} s^{-1}, and seven-day-old seedlings were transferred to soil and grown in a greenhouse under the same conditions. For *AtbZIP59* expression analysis, seven-day-old seedlings were transferred to the callus-inducing medium (CIM, B5 medium supplemented with 0.5 mg l^{-1} 2,4-dichlorophenoxyacetic acid (2,4-D) and 0.05 mg l^{-1} kinetin)[4] for the times indicated. For observation of the callus-forming phenotype of *air1-2*, *lbd16-2* and *air1-2 lbd16-2* mutants, five-day-old seedlings and the cotyledon and hypocotyl explants from seven-day-old seedlings were incubated on CIM for 9 days, and the area of root pericycle or pericycle-derived callus layer of ~1 cm below the root–hypocotyl joint was determined with ImageJ software. For observation of the lateral root formation, five-day-old seedlings were then grown on B5 medium for 5 days. To examine the root response to exogenous auxin, four-day-old WT, *air1-2* and the homozygous *ProAtbZIP59::AtbZIP59–GFP air1-2* seedlings were transferred to solid MS supplemented with various concentrations of 1-naphthylacetic acid (NAA) for 5 days and photographed. Seedlings were then cleared and the number of lateral root initiates was quantified. To observe the callus-forming phenotype, transgenic seedlings harbouring an empty vector, *Pro35S::AtbZIP59–MYC*, *Pro35S::LBD16*, or *Pro35S::FAD-BD* were grown on B5 medium without exogenous phytohormone. For treatment with the protein synthetic inhibitor cycloheximide (CHX) or the proteasome inhibitor MG132, seven-day-old *ProAtbZIP59::AtbZIP59–GFP air1-2* seedlings were transferred to liquid B5 medium or CIM with or without 1 μM CHX or 20 mM MG132 for 48 h. All of the above analyses were performed with at least three independent biological replicates.

Plasmid construction and *Arabidopsis* transformation. A genomic *AtbZIP59* DNA fragment containing a 1,907-base-pair (bp) promoter and a 1,194-bp coding region was fused with a *GFP* sequence and cloned into the pCAMBIA1300 plasmid (Cambia) to generate *ProAtbZIP59::AtbZIP59–GFP*. The *ProLBD16::LBD16–GFP* construct was generated by fusion of the amplified 2,067-bp promoter and the 735-bp coding region of *LBD16* in-frame with *GFP* in the pME18 plasmid. To generate the *ProAtbZIP59::GUS* construct, the 1,907-bp promoter region of *AtbZIP59* was cloned upstream of the *GUS* gene in the pCAMBIA1300 plasmid. For generation of the *Pro35S::AtbZIP59–MYC*, *Pro35S::LBD16* and *Pro35S::FAD-BD* constructs, cDNA fragments of *AtbZIP59*, *LBD16* and *FAD-BD* were cloned, respectively, into the pVIP96 or pVIPMYC binary vectors[36]. To generate the *Super::LBD16–FLAG* construct, cDNA fragments of *LBD16* were cloned into a modified Super1300 vector[37]. A six-glycine linker sequence was inserted upstream of the GFP, MYC or FLAG tag to minimize the influence of the tag on the target protein and optimize the stability of the target protein[38,39]. All primers used for the generation of the constructs are listed in Supplementary Table 1.

All plasmids were introduced into the *Agrobacterium tumefaciens* strain ABI or EHA105 and transformed into *Arabidopsis* Columbia-0 (Col-0) using the floral dip method[40] to generate transgenic plants. At least ten independent transgenic lines with a single T-DNA insertion were generated for each construct, and T3 homozygotes of at least three lines were used for subsequent experiments.

Gene expression analyses. Quantitative RT–PCR was conducted as described previously[15], and the relative expression level of each gene was calculated using the ΔΔCT (cycle threshold) method, and *ACTIN7* was used as an internal control[41]. All qRT–PCR analyses were performed with three independent biological replicates. All primers used in this study are listed in Supplementary Table 1. The histochemical GUS staining assay was performed as described previously[36]. Briefly, five-day-old *ProAtbZIP59::GUS* transgenic seedlings before and after incubation on CIM for 96 h were stained in a 37 °C incubator for 30 min.

Confocal microscopy. To visualize the expression of AtbZIP59–GFP, LBD16–GFP and root meristem markers, the root or other organ samples were mounted in 10 mg l^{-1} propidium iodide (Sigma) and imaged using an Olympus FV1000-MPE laser scanning microscope. A GFP excitation/emission filter (488 nm/525 nm) was used to visualize the gene-specific fluorescence. The propidium iodide signal was visualized by excitation with an argon laser at 488 nm and a spectral detector set at > 585 nm for the emission.

Yeast two-hybrid assays. For yeast two-hybrid screening, the RNAs isolated from ten-day-old seedlings incubated on CIM for 12, 24 and 48 h were used to construct a yeast two-hybrid cDNA library. Yeast two-hybrid assays were carried out with LBD17 as a bait, based on the ProQuest two-hybrid system (Invitrogen) in the presence of 50 mM 3-amino1,2,4-triazol (3-AT)[42], which can effectively repress the background transcription activation activity of full-length LBD17. To verify the interaction between AtbZIP59 and LBD17, the full-length coding sequence of *AtbZIP59* was cloned into *pDEST22* as prey, and that of *LBD17* was cloned into *pDEST32* (Invitrogen). The interaction of AtbZIP59 and LBD17 was tested in the yeast strain Mav203 (Invitrogen) on a SC-Leu-Trp plate and assayed by X-Gal (5-bromo-5-chloro-3-indolyl-β-D-galactoside) staining after 2 h of incubation at 37 °C. The primers for amplifying *AtbZIP59* and *LBD17* cDNAs for yeast two-hybrid constructs are listed in Supplementary Table 1.

Co-immunoprecipitation (co-IP) assay. To examine the interaction of AtbZIP59 and LBDs in planta, the coding sequences of *AtbZIP59*, *LBD16*, *LBD17* and *LBD29* fused with a six-glycine linker and a GFP or MYC tag sequence were cloned into a modified Super1300 vector[37–39]. All primers used for the generation of the constructs are listed in Supplementary Table 1. The transient expression assays were performed with four-week-old *N. benthamiana* plants as described previously[43]. Briefly, *N. benthamiana* leaves were infiltrated with *Agrobacterium tumefaciens* strains harbouring *Super::LBD16–GFP* (*LBD16–GFP*), *Super::LBD17–GFP* (*LBD17–GFP*) or *Super::LBD29–GFP* (*LBD29–GFP*) and/or *Super::AtbZIP59–MYC* (*AtbZIP59–MYC*) constructs, respectively. At 72 h after infiltration, 2 g of *Agrobacterium*-infiltrated leaves were collected, and total protein was extracted and then incubated with the agarose-conjugated anti-GFP matrix (Abmart) for 4 h with rotation at 4 °C. After washing three times with 1 ml of immunoprecipitation buffer, the agarose beads were denatured in 50 μl of SDS loading buffer. The samples were separated by SDS–polyacrylamide gel electrophoresis and immunoblotted with the corresponding antibody.

Co-IP assays of *Arabidopsis* were performed as described above. To test the effect of CIM on the interaction of AtbZIP59 and LBD16 in stable transgenic *Arabidopsis* plants, ten-day-old homozygous *Pro35S::AtbZIP59–MYC* and *Pro35S::AtbZIP59–MYC Super::LBD16–FLAG* seedlings were incubated on CIM or hormone-free B5 medium for 48 h. Then, 5 g of seedlings were collected and lysed for the Co-IP experiments. The agarose-conjugated anti-MYC beads (Abmart) were used for the affinity binding of the AtbZIP59–MYC fusion protein and anti-MYC–HRP (Abmart) was used to detect the MYC epitope and anti-FLAG antibody was used to detect the FLAG epitope. Each co-IP experiment was repeated at least three times.

Bimolecular fluorescence complementation assays. Full-length coding sequences of *LBD16*, *LBD17* and *LBD29* were respectively cloned into the binary vector pSPYNE-35S to generate the N-terminal half of the YFP-fused LBD constructs, and the full-length coding sequence of *AtbZIP59* was cloned into the vector pSPYCE–35S to generate the C-terminal half of the YFP-fused AtbZIP59 construct[25] using the restriction enzymes XbaI and XhoI. Similarly, a six-glycine linker sequence was inserted upstream of the YFP tag. Primers for the constructions are listed in Supplementary Table 1. The resulting constructs were then introduced into the *Agrobacterium strain* EHA105. Bimolecular fluorescence complementation analysis was performed as described previously[25] with some modifications. The *Agrobacterium* harbouring *LBD16–YFP^N*, *LBD17–YFP^N* or *LBD29–YFP^N* was co-infiltrated with pCam–P19 and *AtbZIP59–YFP^C* into the leaves of *N. benthamiana* plants. Co-infiltration of the empty vector pSPYNE–35S and the *AtbZIP59–YFP^C* construct or pSPYCE–35S and the *LBD16–YFP^N*, *LBD17–YFP^N* and *LBD29–YFP^N* constructs was used as a negative control. The interaction of GIF2 and GRF1 was used as a positive control[44]. After incubation in the dark for 24 h and then in light for 72 h, the leaves were dissected and visualized under an Olympus FV1000-MPE laser scanning microscope.

Chromatin immunoprecipitation (ChIP)–qPCR assays. ChIP assays were performed according to a published protocol[45] with minor modifications. Briefly, 1.5 g of ten-day-old *ProLBD16::LBD16–GFP lbd16-2*, *ProAtbZIP59::AtbZIP59–GFP air1-2* and WT seedlings cultured in liquid CIM for 36 h were crosslinked in 1% formaldehyde and their chromatin was isolated. GFP antibody (Abcam) was used to immunoprecipitate the protein–DNA complex, and the precipitated DNA was purified for qPCR analysis. Chromatin precipitated without antibody was used as a negative control, while the isolated chromatin before precipitation was used as an input control. Primers used for ChIP–qPCR are listed in Supplementary Table 1. The ChIP–qPCRs were performed with three biological and technical replicates and WT plants were used as a control.

Transient transcriptional activity assay. For the transient transcriptional activity assay in the *Arabidopsis* protoplast, a 1,020-bp *Arabidopsis* genomic DNA fragment upstream of the *FAD-BD* translation start site was amplified by PCR and cloned in upstream of LUC into TQ379[46], which harbours the Pro35S:REN (*Renilla*) cassette, to create the reporter *ProFAD-BD::LUC*. The coding sequences of *LBD16* and *AtbZIP59* fused with a six-glycine linker and a GFP tag sequence were respectively cloned into the p326–35S–cGFP vector as effectors[47]. The Ω translational enhancer[48,49] was cloned upstream of *LBD16* or *AtbZIP59* to increase their final expression levels. All primers used for the generation of the constructs are listed in Supplementary Table 1.

For the dual-luciferase reporter assay, *Arabidopsis* protoplasts were prepared using three-week-old *Arabidopsis* (Col-0) leaves according to a published protocol[50]. After transfection, the protoplasts were cultured at 22 °C in the light for 4 h and then in the dark for 14 h. The protoplasts were then lysed with passive lysis buffer (Promega; E1910). LUC and REN activities were quantified and measured with a luminometer (Promega GloMax Multi Jr). LUC activity was calculated by normalizing to that of REN. Three independent experiments (biological triplicates) were performed.

Life Sciences Reporting Summary. Further information on experimental design is available in the Life Sciences Reporting Summary.

Data availability. The data that support the findings of this study are available from the corresponding authors upon request. Sequence data in this article can be found in the *Arabidopsis* Genome initiative or GenBank/EMBL databases under the following accession numbers: *LBD16* (At2g42430), *LBD17* (At2g42440), *LBD29* (At3g58190), *AtbZIP59* (At2g31370), *WOX5* (At3g11260), *PLT1* (At3g20840), *FAD-BD* (At1g30760), *ACTIN7* (At5g09810), *UBIQUITIN10* (At3g52590) and *GPAC* (At3g04120).

Received: 22 October 2017; Accepted: 20 December 2017;
Published online: 22 January 2018

References

1. Birnbaum, K. D. & Sanchez Alvarado, A. Slicing across kingdoms: regeneration in plants and animals. *Cell* **132**, 697–710 (2008).
2. Sugimoto, K., Gordon, S. P. & Meyerowitz, E. M. Regeneration in plants and animals: dedifferentiation, transdifferentiation, or just differentiation? *Trends Cell. Biol.* **21**, 212–218 (2011).
3. Skoog, F. & Miller, C. O. Chemical regulation of growth and organ formation in plant tissues cultured *in vitro*. *Symp. Soc. Exp. Biol.* **54**, 118–130 (1957).
4. Valvekens, D., Montagu, M. V. & Van Lijsebettens, M. *Agrobacterium tumefaciens*-mediated transformation of *Arabidopsis thaliana* root explants by using kanamycin selection. *Proc. Natl Acad. Sci. USA* **85**, 5536–5540 (1988).
5. Gordon, S. P. et al. Pattern formation during *de novo* assembly of the *Arabidopsis* shoot meristem. *Development* **134**, 3539–3548 (2007).

6. Chandler, J. W. Founder cell specification. *Trends Plant Sci.* **16**, 607–613 (2011).
7. Ahmad, P. et al. Role of transgenic plants in agriculture and biopharming. *Biotechnol. Adv.* **30**, 524–540 (2012).
8. Viacheslavova, A. O. et al. Expression of heterologous genes in plant systems: new possibilities. *Genetika* **48**, 1245–1259 (2012).
9. Atta, R. et al. Pluripotency of *Arabidopsis* xylem pericycle underlies shoot regeneration from root and hypocotyl explants grown *in vitro*. *Plant J.* **57**, 626–644 (2009).
10. Sugimoto, K., Jiao, Y. & Meyerowitz, E. M. *Arabidopsis* regeneration from multiple tissues occurs via a root development pathway. *Dev. Cell.* **18**, 463–471 (2010).
11. Che, P., Lall, S. & Howell, S. H. Developmental steps in acquiring competence for shoot development in *Arabidopsis* tissue culture. *Planta* **226**, 1183–1194 (2007).
12. Laplaze, L. et al. GAL4-GFP enhancer trap lines for genetic manipulation of lateral root development in *Arabidopsis thaliana*. *J. Exp. Bot.* **56**, 2433–2442 (2005).
13. Okushima, Y., Fukaki, H., Onoda, M., Theologis, A. & Tasaka, M. ARF7 and ARF19 regulate lateral root formation via direct activation of *LBD/ASL* genes in *Arabidopsis*. *Plant Cell.* **19**, 118–130 (2007).
14. Lee, H. W., Kim, N. Y., Lee, D. J. & Kim, J. *LBD18/ASL20* regulates lateral root formation in combination with *LBD16/ASL18* downstream of ARF7 and ARF19 in *Arabidopsis*. *Plant Physiol.* **151**, 1377–1389 (2009).
15. Fan, M., Xu, C., Xu, K. & Hu, Y. LATERAL ORGAN BOUNDARIES DOMAIN transcription factors direct callus formation in *Arabidopsis* regeneration. *Cell. Res.* **22**, 1169–1180 (2012).
16. Rosspopoff, O. et al. Direct conversion of root primordium into shoot meristem relies on timing of stem cell niche development. *Development* **144**, 1187–1200 (2017).
17. Iwase, A. et al. The AP2/ERF transcription factor WIND1 controls cell dedifferentiation in *Arabidopsis*. *Curr. Biol.* **21**, 508–514 (2011).
18. Ikeuchi, M. et al. Wounding triggers callus formation via dynamic hormonal and transcriptional changes. *Plant Physiol.* **175**, 1158–1174 (2017).
19. Jakoby, M. et al. bZIP transcription factors in *Arabidopsis*. *Trends Plant Sci.* **7**, 106–111 (2002).
20. Deppmann, C. D. et al. Dimerization specificity of all 67 B-ZIP motifs in *Arabidopsis thaliana*: a comparison to *Homo sapiens* B-ZIP motifs. *Nucleic Acids Res.* **32**, 3435–3445 (2004).
21. Vinson, C. R., Sigler, P. B. & McKnight, S. L. Scissors-grip model for DNA recognition by a family of leucine zipper proteins. *Science* **246**, 911–916 (1989).
22. Ellenberger, T. E., Brandl, C. J., Struhl, K. & Harrison, S. C. The GCN4 basic region leucine zipper binds DNA as a dimer of uninterrupted alpha helices: crystal structure of the protein-DNA complex. *Cell* **71**, 1223–1237 (1992).
23. Tsugama, D., Liu, S. & Takano, T. Analysis of functions of VIP1 and its close homologs in osmosensory responses of *Arabidopsis thaliana*. *PLoS ONE* **9**, e103930 (2014).
24. Van Oosten, M. J., Sharkhuu, A., Batelli, G., Bressan, R. A. & Maggio, A. The *Arabidopsis thaliana* mutant *air1* implicates SOS3 in the regulation of anthocyanins under salt stress. *Plant Mol. Biol.* **83**, 405–415 (2013).
25. Walter, M. et al. Visualization of protein interactions in living plant cells using bimolecular fluorescence complementation. *Plant J.* **40**, 428–438 (2004).
26. Daniel, B. et al. Oxidation of monolignols by members of the berberine bridge enzyme family suggests a role in plant cell wall metabolism. *J. Biol. Chem.* **290**, 18770–18781 (2015).
27. Lee, H. W., Kim, M. J., Kim, N. Y., Lee, S. H. & Kim, J. LBD18 acts as a transcriptional activator that directly binds to the *EXPANSIN14* promoter in promoting lateral root emergence of *Arabidopsis*. *Plant J.* **73**, 212–224 (2013).
28. Xu, K. et al. A genome-wide transcriptome profiling reveals the early molecular events during callus initiation in *Arabidopsis* multiple organs. *Genomics* **100**, 116–124 (2012).
29. Heyman, J. et al. The heterodimeric transcription factor complex ERF115–PAT1 grants regeneration competence. *Nat. Plants* **2**, 16165 (2016).
30. Zhong, L. P. et al. Overexpression of insulin-like growth factor binding protein 3 in oral squamous cell carcinoma. *Oncol. Rep.* **20**, 1441–1447 (2008).
31. Rizzino, A. & Wuebben, E. L. Sox2/Oct4: A delicately balanced partnership in pluripotent stem cells and embryogenesis. *Biochim. Biophys. Acta* **1859**, 780–791 (2016).
32. Casimiro, I. et al. Dissecting *Arabidopsis* lateral root development. *Trends Plant Sci.* **8**, 165–171 (2003).
33. Casimiro, I. et al. Auxin transport promotes *Arabidopsis* lateral root initiation. *Plant Cell.* **13**, 843–852 (2001).
34. Aida, M. et al. The *PLETHORA* genes mediate patterning of the *Arabidopsis* root stem cell niche. *Cell* **119**, 109–120 (2004).
35. Haecker, A. et al. Expression dynamics of *WOX* genes mark cell fate decisions during early embryonic patterning in *Arabidopsis thaliana*. *Development* **131**, 657–668 (2004).
36. Hu, Y., Xie, Q. & Chua, N. H. The *Arabidopsis* auxin-inducible gene *ARGOS* controls lateral organ size. *Plant Cell.* **15**, 1951–1961 (2003).
37. Chinnusamy, V. et al. ICE1: a regulator of cold-induced transcriptome and freezing tolerance in *Arabidopsis*. *Genes. Dev.* **17**, 1043–1054 (2003).
38. Funakoshi, M. & Hochstrasser, M. Small epitope-linker modules for PCR-based C-terminal tagging in *Saccharomyces cerevisiae*. *Yeast* **26**, 185–192 (2009).
39. Robinson, C. R. & Sauer, R. T. Optimizing the stability of single-chain proteins by linker length and composition mutagenesis. *Proc. Natl Acad. Sci. USA* **95**, 5929–5934 (1998).
40. Clough, S. J. & Bent, A. F. Floral dip: a simplified method for *Agrobacterium*-mediated transformation of *Arabidopsis thaliana*. *Plant J.* **16**, 735–743 (1998).
41. Livak, K. J. & Schmittgen, T. D. Analysis of relative gene expression data using real-time quantitative PCR and the 2(-Delta Delta C(T)) Method. *Methods* **25**, 402–408 (2001).
42. Bharti, K. et al. Isolation and characterization of HsfA3, a new heat stress transcription factor of *Lycopersicon peruvianum*. *Plant J.* **22**, 355–365 (2000).
43. Voinnet, O., Rivas, S., Mestre, P. & Baulcombe, D. An enhanced transient expression system in plants based on suppression of gene silencing by the p19 protein of tomato bushy stunt virus. *Plant J.* **33**, 949–956 (2003).
44. Kim, J. H. & Kende, H. A transcriptional coactivator, AtGIF1, is involved in regulating leaf growth and morphology in *Arabidopsis*. *Proc. Natl Acad. Sci. USA* **101**, 13374–13379 (2004).
45. Bowler, C. et al. Chromatin techniques for plant cells. *Plant J.* **39**, 776–789 (2004).
46. Zhang, T. Q. et al. A two-step model for *de novo* activation of WUSCHEL during plant shoot regeneration. *Plant Cell.* **29**, 1073–1087 (2017).
47. Lin, X. L. et al. An *Arabidopsis* SUMO E3 ligase, SIZ1, negatively regulates photomorphogenesis by promoting COP1 activity. *PLoS Genet.* **12**, e1006016 (2016).
48. Gallie, D. R. & Kado, C. I. A translational enhancer derived from tobacco mosaic virus is functionally equivalent to a Shine-Dalgarno sequence. *Proc. Natl Acad. Sci. USA* **86**, 129–132 (1989).
49. Gallie, D. R., Lucas, W. J. & Walbot, V. Visualizing mRNA expression in plant protoplasts: factors influencing efficient mRNA uptake and translation. *Plant Cell.* **1**, 301–311 (1989).
50. Yoo, S. D., Cho, Y. H. & Sheen, J. *Arabidopsis* mesophyll protoplasts: a versatile cell system for transient gene expression analysis. *Nat. Protoc.* **2**, 1565–1572 (2007).

Acknowledgements

We are grateful to B. Scheres, J. Haseloff, N.-H. Chua, J.-W. Wang and J. Jin for providing the seeds and constructs used in this study. We thank J. M. Alonso (North Carolina State University) for critical comments on the manuscript. We acknowledge K. Yang for help in preparing some of the constructs for the co-IP experiment. This work was supported by the National Natural Science Foundation of China (grant no. 31230009 and grant no. 31771632), the Ministry of Science and Technology of China (grant no. 2013CB967300) and the Strategic Priority Research Program of Chinese Academy of Sciences (grant no. XDPB0403).

Author contributions

Y.H. conceived the project; C.X. and Y.H. designed the experiments; C.X., H.C., H.W. and W.X. performed the experiments; Q.Z., E.X., S.Z., R.Y. and D.Y. contributed to the generation of some constructs; C.X. and Y.H. analysed the data and wrote the manuscript.

Competing interests

The authors declare no competing financial interests.

Additional information

Supplementary information accompanies this paper at https://doi.org/10.1038/s41477-017-0095-4.

Reprints and permissions information is available at www.nature.com/reprints.

Correspondence and requests for materials should be addressed to Y.H.

Publisher's note: Springer Nature remains neutral with regard to jurisdictional claims in published maps and institutional affiliations.

nature research

Corresponding author(s): Yuxin Hu

☒ Initial submission ☐ Revised version ☐ Final submission

Life Sciences Reporting Summary

Nature Research wishes to improve the reproducibility of the work that we publish. This form is intended for publication with all accepted life science papers and provides structure for consistency and transparency in reporting. Every life science submission will use this form; some list items might not apply to an individual manuscript, but all fields must be completed for clarity.

For further information on the points included in this form, see Reporting Life Sciences Research. For further information on Nature Research policies, including our data availability policy, see Authors & Referees and the Editorial Policy Checklist.

Experimental design

1. Sample size

Describe how sample size was determined. | Sample size has been described in the statistic source data file.

2. Data exclusions

Describe any data exclusions. | No exclusion of the data was performed in this study.

3. Replication

Describe whether the experimental findings were reliably reproduced. | All experimental findings were reliably reproduced.

4. Randomization

Describe how samples/organisms/participants were allocated into experimental groups. | There is no allocation of samples into group in our study.

5. Blinding

Describe whether the investigators were blinded to group allocation during data collection and/or analysis. | There is no allocation of samples into groups.

Note: all studies involving animals and/or human research participants must disclose whether blinding and randomization were used.

6. Statistical parameters

For all figures and tables that use statistical methods, confirm that the following items are present in relevant figure legends (or in the Methods section if additional space is needed).

n/a	Confirmed	
☐	☒	The exact sample size (*n*) for each experimental group/condition, given as a discrete number and unit of measurement (animals, litters, cultures, etc.)
☐	☒	A description of how samples were collected, noting whether measurements were taken from distinct samples or whether the same sample was measured repeatedly
☐	☒	A statement indicating how many times each experiment was replicated
☐	☒	The statistical test(s) used and whether they are one- or two-sided (note: only common tests should be described solely by name; more complex techniques should be described in the Methods section)
☒	☐	A description of any assumptions or corrections, such as an adjustment for multiple comparisons
☒	☐	The test results (e.g. *P* values) given as exact values whenever possible and with confidence intervals noted
☐	☒	A clear description of statistics including central tendency (e.g. median, mean) and variation (e.g. standard deviation, interquartile range)
☐	☒	Clearly defined error bars

See the web collection on statistics for biologists for further resources and guidance.

Software

Policy information about availability of computer code

7. Software

Describe the software used to analyze the data in this | The multiple comparisons of statistical analysis were performed with the software

study.

SPSS 20 (https://www.ibm.com/support/knowledgecenter/en/SSLVMB_20.0.0/com.ibm.spss.statistics_20.kc.doc/pv_welcome.html);
The fluorescence signals were processed and integrated using the ImageJ software (https://imagej.nih.gov/ij/);
Callus area was determined with the ImageJ software.

For manuscripts utilizing custom algorithms or software that are central to the paper but not yet described in the published literature, software must be made available to editors and reviewers upon request. We strongly encourage code deposition in a community repository (e.g. GitHub). *Nature Methods* guidance for providing algorithms and software for publication provides further information on this topic.

Materials and reagents

Policy information about availability of materials

8. Materials availability

Indicate whether there are restrictions on availability of unique materials or if these materials are only available for distribution by a for-profit company.

No unique materials were used.

9. Antibodies

Describe the antibodies used and how they were validated for use in the system under study (i.e. assay and species).

The anti-GFP antibody (Code M048-3), the anti-MYC antibody (Code M047-3), the anti-FLAG antibody (Code M185-3L), the anti-ACTIN antibody (Code M177-3), the anti-GFP mAB-Agarose (Code D153-8) and the anti-MYC mAB-Agarose (Code M047-8) for western blotting or CO-IP assays were purchased from MBL. The details of the production were described in the previous publications [Asada et al. (2010) J. Neurosci. 30, 8852-8865; Tani et al. (2012) RNA Biol. 9, 1370--1379; Lee et al. (2017) Cancer Letters 403,144-151; Vandekerckhove et al. (1978) PNAS 75, 1106; Obuse et al. (2004) Nat. Cell Biol. 6, 1135-1141; Sun et al. (2011) J. Biol. Chem. 286, 4226-4235].
The anti-GFP antibody for ChIP-qPCR assays was purchased from Abcam (code ab290) and was validated in Wang et al. (2016) Nature Commun. 18, 6:8822.

10. Eukaryotic cell lines

a. State the source of each eukaryotic cell line used.

N/A

b. Describe the method of cell line authentication used.

N/A

c. Report whether the cell lines were tested for mycoplasma contamination.

N/A

d. If any of the cell lines used are listed in the database of commonly misidentified cell lines maintained by ICLAC, provide a scientific rationale for their use.

N/A

Animals and human research participants

Policy information about studies involving animals; when reporting animal research, follow the ARRIVE guidelines

11. Description of research animals

Provide details on animals and/or animal-derived materials used in the study.

N/A

Policy information about studies involving human research participants

12. Description of human research participants

Describe the covariate-relevant population characteristics of the human research participants.

N/A